Holographic Projection for Multi-spot Structured Illumination Microscopy

EDWARD N. WARD,[1] ROBERT PAL,[1,*]

[1]*Department of Chemistry, Durham University, South Road, Durham, DH1 3LE, UK*

*robert.pal@dur.ac.uk

Abstract: This paper describes the design and testing of a multi-spot structured illumination microscopy system using computer-generated holograms to create the required excitation patterns. Furthermore, it demonstrates the use of an adapted direct search algorithm for calculating the holograms that allows for imaging across an extended field of view. The system was tested on fixed targets and live cells yielding a two times resolution increase over conventional diffraction-limited imaging.

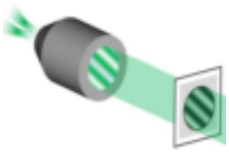

We present the design and testing of a multi-spot structured illumination microscopy system using computer-generated holograms to create the required excitation patterns. It demonstrates the use of an adapted direct search algorithm for calculating the holograms that allows for imaging across an extended field of view. The system was tested on fixed targets and live cells yielding a two times resolution increase over conventional diffraction-limited imaging.

The results here demonstrate that holography provides an efficient means of pattern projection for MSIM imaging. It provides a significant improvement in the efficiency of pattern projection and more importantly it allows for the testing of more diverse excitation patterns than possible with amplitude-only projection. For example, PSF engineering using phase modulation can be easily incorporated into the calculated holograms, potentially generating sub-diffraction structures in the excitation pattern. The ability to incorporate PSF engineering into SIM opens up holographic MSIM as a potential method for further increasing resolution with little or no change to the imaging system.

This article has been accepted for publication and undergone full peer review but has not been through the copyediting, typesetting, pagination and proofreading process, which may lead to differences between this version and the Version of Record. Please cite this article as doi: 10.1111/jmi.12787

1. Introduction

Structured Illumination Microscopy (SIM) is one of the most widely used super-resolution techniques in microscopy. The principle behind the technique is that high spatial frequencies of the sample structure can be recorded by shifting a known excitation pattern over the sample.[1] The high frequency information is extracted from a stack of images acquired with different orientations of the pattern. Multi-spot SIM (MSIM) is a variant on the SIM method which uses arrays of spots as the excitation patterns.[2,3] While MSIM requires significantly more pattern shifts to acquire a single super-resolution image, it has the advantage over striped-pattern SIM that it is invariant to polarisation and is simpler to implement as no moving parts are required in the excitation optics. The multi-spot patterns also allow for digital pinholling approaches to reduce out-of-focus blur in the acquired images, improving imaging performance deeper into tissues. Traditionally, the spot patterns required for MSIM were generated using a Digital Micromirror Device (DMD) operating as an amplitude-only Spatial Light Modulator (SLM). While easy to implement, the efficiency of generating the spot patterns this way is exceptionally low, with typically fewer than 1% of pixels switched on at any one time. Furthermore, in this configuration the uniformity of the excitation pattern at the focal plane is proportional to the uniformity of the illumination of the SLM. In most systems to-date, this means that perfect uniformity is difficult to accomplish, and that imaging must be confined to a region of the FOV where pseudo-uniform illumination can be achieved. Holography offers a new way to generate the required spot patterns in the focal plane with a significantly higher efficiency and uniformity.[4,5] By modulating the

phase of a coherent beam entering a lens, it is possible to generate any desired intensity pattern in the focal plane. This is typically used in optical trapping, where a few high intensity spots are required to trap and move small particles.[6] If changing patterns are required, the phase change is applied to the pupil plane of an objective lens using a phase-only liquid-crystal SLM, and the required phase pattern is updated dynamically after being calculated computationally using a phase-retrieval algorithm. Based on this technology, an MSIM system was constructed using computer-generated holograms to create the multi-spot patterns in the focal plane. The system was tested on fixed cells, yielding a two times resolution increase over diffraction-limited imaging, comparable with current MSIM techniques. In addition, a method is demonstrated to incorporate correction for aberrations that vary across the field of view to further improve imaging. Furthermore, this technique opens the path to further improve imaging by using a range of patterns with engineered excitation patterns.[7]

2. Methods

2.1 Optical setup

The apparatus used is shown in Fig. 1. Two 488 nm and 532 nm lasers (Roithner RLS4116 & CW532-050F, Austria) are focused through a single-mode fibre (Thor Labs P1-405B, US) acting as a spatial filter. The beam is collimated by a lens (Thor Labs LA1134, US) before passing through a linear polariser (Thor Labs LPVISE100, US), quarter waveplate (Thor Labs AHWP05M, US) and a liquid-crystal SLM (Sony LCX080, Japan). The beam then passes through a second linear polariser (Thor Labs LPVISE100, US) and quarter waveplate (Thor Labs AHWP05M, US). An image of the SLM is then relayed onto the back of the objective lens by two relay lenses (Thor Labs

LB1437, US) through a long-pass dichroic (Leica Microsystems I3 & N2.1, Germany) inside a microscope chassis (Leica Microsystems DMi8, Germany). A 100X 1.4 numerical aperture oil-immersion objective was used for all imaging (Leica Microsystems 11506372, Germany). The focal lengths of the relay and tube lens are equal, giving a 1x magnification of the image of the SLM. The fluorescent signal is isolated with an emission filters (Leica Microsystems I3 & N2.1, Germany) and imaged on an electron-multiplying charge-coupled device (Andor iXon 888, UK). The hardware was controlled through MATLAB and LabVIEW programs.

2.2 Hologram calculation

Holograms were calculated using an adapted Direct Search (DS) approach, optimising the hologram on a pixel-by-pixel basis.[8] Computationally, the amplitude at any point in the focal plane $\epsilon(\vec{r})$ can be calculated as the sum of the contributions from the *N* pixels in the plane of the SLM:[9]

$$\varepsilon(\vec{r}) = \sum_{i=0} A_0(\vec{\rho}_i)\exp(i\varphi(\vec{\rho}_i))\kappa(\vec{r},\vec{\rho}_i)\exp\left(-i\frac{2\pi\vec{r}\cdot\vec{\rho}_i}{\lambda f}\right) \qquad (1)$$

$A_0(\vec{\rho}_i)$ and $\phi(\vec{\rho}_i)$ denote the amplitude and phase of the light incident on the ith pixel on the SLM at a point $\vec{\rho}$. λ is the wavelength of the light and f is focal length of the optical train. Assuming the light incident on the SLM has the same phase, $\phi(\vec{\rho})$ represents the phase change imparted by the SLM. The goal of holography is to calculate the optimal values for $\phi(\vec{\rho})$ to generate the desired light pattern in the focal plane. For each pixel on the SLM, the direct search algorithm calculates the value of ε at each spot location and chooses a value for $\varphi(\vec{\rho})$ that maximises the uniformity and the sum of the intensities of

the spots. $K(\vec{r},\vec{\rho})$ is a kernel which can be used to change the shape of the PSF at the focal point.

To properly correct for pattern aberrations, a modified DS algorithm was generated, introducing a value for $K(\vec{r},\vec{\rho})$ to compensate for location-dependent aberrations. As an example, in this work the most significant location-dependent aberration was a radially varying astigmatism which increased with the distance from the centre of the grid. As such, the kernel was set to

$$K\left(\vec{r},\vec{\rho}\right)=\exp\left(i\left(\vec{r}\cdot\vec{r}\right)\left(\alpha\rho_x\rho_y\cdot\cos\left(\theta_r\right)+\beta\left(\rho_x^2-\rho_y^2\right)\cdot\cos\left(\theta_r\right)\right)\right) \quad (2)$$

Here, α and β are constants describing the magnitude of the first two astigmatisms as defined by the Zernike polynomials. The $\cos(\theta_r)$ and $\sin(\theta_r)$ dependence describe the change in the 'direction' of the astigmatism around the centre of the grid. Although in this work only astigmatism was built into the DS algorithm, it would be possible to extend the kernel to account for a greater number of variable aberrations. Given the large number of iterations required for convergence, hologram calculation typically takes one minute for a 700x700 pixel hologram. While such long calculation times would prevent the use of the algorithm in dynamic applications, in MSIM the patterns are constant and the holograms can be computed in advance of imaging and loaded from memory. The hologram calculation was performed in MATLAB and accelerated with Graphical Processor Unit (GPU) (NVIDIA 1050-Ti, US) processing. The phase modulation of the SLM was previously measured using a common path interferometer to build a look-up table to ensure optimal hologram projection. Finally, before projection of the holograms, a global aberration correction phase mask was added to the hologram, compensating for aberrations which were constant across the pattern. A

different hologram and global aberration correction phase mask was calculated for each of the excitation wavelengths used, allowing for achromatic pattern projection with no modification to the optics. Fig. 2 shows an example of the effects of aberration correction on the MSIM patterns generated. Apparent in the uncorrected pattern is the need to include aberration correction in the hologram calculation model. In comparison to the corrected pattern, the contrast of the pattern has been reduced across the FOV and aberrations which mis-shape the PSFs are more significant in the upper left corner than the lower right.

2.3 Image processing

Before super-resolution reconstruction, the excitation patterns were estimated through an adaptation of a previously described method.[7] Briefly, this is an iterative process, minimising the difference between the predicted and gathered images under estimates of the excitation patterns. This estimation approach was used to determine the excitation patterns in live and fixed cell samples. Post-acquisition pattern estimation is preferable to using pre-calibrated patterns since it is less susceptible to sample-specific variance. However, estimation is impossible in sparse samples, and in such cases a pre-acquisition calibration was required. This requirement to use pre-calibrated patterns arises from the pattern spacing estimation method used in the estimation algorithm. For reliable estimation, this step requires a sample density high enough that in each acquired frame there are at least four adjacent excitation spots visible. Higher sample densities are also required when imaging samples consisting of sparse point-emitters, since these can be misidentified by the algorithm as displaced excitation spots. Pre-calibrated patterns were determined by estimating the patterns projected onto a

fluorescent Rhodamine 6G monolayer and then loading this ideal pattern for image reconstruction. After pattern estimation, acquired images were then digitally pinholed by excluding light from outside the region of the focal spots.

From the image data and estimated patterns, super-resolution images were reconstructed through a combination of the joint Richardson-Lucy (JRL) algorithm and the Pattern-Illuminated Fourier Ptychography (PIFP) algorithm. While each of these algorithms on their own is capable of reconstructing the super-resolution image, the combination of the two algorithms has been shown to give the best results on a broad range of underlying sample structures.[10] For example, PIFP reconstruction generally performs better on filament-like structures and JRL on point-emitters. Here, a sequential approach to reconstruction was used, seeding the JRL reconstruction process with the result of the PIFP reconstruction. All image processing was completed in MATLAB and, where possible, accelerated using the GPU.

2.4 Imaging

To determine the constants for aberration correction, un-corrected patterns were projected onto a Rhodamine 6G fluorescent monolayer. The change in aberrations across the field of view was calculated by measuring the magnitude of the aberrations at each corner of the excitation grid. Global aberration-corrections, for aberrations constant across the field of view, were simultaneously determined. For all imaging, the most significant aberration was a radially-dependent astigmatism, as well as a global spherical aberration. This was corrected for by generating new holograms for aberration-free patterns. This process was then repeated for both excitation wavelengths used, as each colour will have slightly different aberrations present: a

result of chromatic aberrations in the optical train. For cell imaging, NIH/3T3 mouse skin fibroblast cells (American type culture collection, US) were grown onto coverslips and cultured in Dulbecco's modified Eagle's medium (Thermo Fisher 10313021, US) with phenol red. To stain the mitochondrial network, cells were incubated with Mito-tracker Green (MTG) (Thermo Fisher M7514, US). Live-cell imaging was performed in culture media without the use of phenol red. MTG was excited with the 488 nm laser and fluorescence signal detected after a 500 nm long-pass filter. To image the cytoskeleton, NIH/3T3 cells were first fixed with paraformaldehyde and permeabilised using Triton-X 100. Actin filaments were stained in a solution containing AlexaFluor 488-Phalloidin (Thermo Fisher A12379, US) and foetal bovine serum to minimise non-specific staining. The label was excited using a 488 nm laser, and fluorescence signal was detected after a 500 nm long-pass filter. Fixed cells were then mounted with anti-fade mounting media. To measure the performance on point emitters, 100 nm fluorescent beads (Thermo Fisher T7284, US) were dried onto a coverslip and mounted with anti-fade mounting media. Beads were excited using a 532 nm laser, and the fluorescence signal was recovered after a 560 nm long-pass filter.

3. Results

3.1 Fluorescent beads

Fig. 3 shows the results of imaging 100 nm green fluorescent beads mounted sparsely on the surface of a coverslip. Analysis of the full-width half-maxima of the beads, as well as measurements of the distance between resolvable beads, demonstrates at least a doubling of resolution over the diffraction-limited image, in line with the theoretical predictions.[11] The quality of the reconstruction also demonstrates the efficacy of the pre-

calibration pattern estimation. The pre-calibrated patterns have likely performed well on this sample, as both the monolayer and beads lie on the surface of the coverslip, meaning there is similar sample-specific pattern disruption.

3.2 Fixed-cell Imaging

While the fluorescent beads offer an effective way to make quantitative measurements of resolution increase, they are not representative of typical biological structures. To demonstrate the effectiveness of the technique on cellular structures, imaging was conducted on fixed cells. Fig. 4 shows imaging results of labelled actin filaments in fixed cells. Qualitatively, it is clear that resolution has been increased compared to the diffraction-limited imaging.

3.3 Live-cell Imaging

As a final demonstration of the capabilities of this technique, imaging was performed in densely-labelled live cells. Fig. 5 and Fig. 6 show the results of imaging the mitochondrial network in live cells. The mitochondrial network poses a particularly challenging target, as the high density of mitochondria around the cell nucleus greatly increases the amount of background fluorescence. In these conditions, and imaging deeper into tissues, MSIM typically outperforms striped-pattern SIM, as there is less disruption to the excitation patterns, and digital pinholing allows for simple removal of background signal.

4. Discussion

The results here demonstrate that holography provides an efficient means of pattern projection for MSIM imaging. As a technique, this has several advantages over

traditional amplitude-only SLMs. As with any structured-illumination technique, MSIM is susceptible to aberrations in the reconstructed image resulting from imperfect pattern projection. By generating the patterns using phase-engineering of the excitation light, these aberrations can be easily corrected for by modification of the hologram. As an example, many SIM systems are limited by the change in focus when switching between wavelengths. In holographic projection this aberration appears as a change in the focal depth of the excitation pattern between wavelengths. Correcting for this allows for rapid changing between excitation wavelengths without the need for costly achromatic optics or mechanical movement of focusing lenses. Furthermore, holography also allows for the correction of aberrations which vary across the field of view, something not possible with other pattern projection techniques. To this end, we have developed an algorithm to generate the required holograms incorporating varying aberration correction. All of this software is freely available upon request to the authors. Finally, holography provides a significant improvement in the efficiency of pattern projection. The efficiency of the calculated holograms and imperfect performance of the SLM result in a total efficiency of ~20%. While low, this is a considerable improvement over amplitude-only implementations, where only 0.4% of the light incident on the SLM is used at any one time. This greatly-increased efficiency means that holography also allows for more cost-effective lower power lasers to be used as the excitation source.

In addition to these advantages, SIM pattern projection using holography also allows for the testing of more diverse excitation patterns than possible with amplitude-only projection. For example, PSF engineering using phase modulation can be easily incorporated into the calculated holograms, potentially generating sub-diffraction

structures in the excitation pattern.[7,12] The ability to incorporate PSF engineering into SIM opens up holographic MSIM as a potential method for further increasing resolution with little or no change to the system.

Despite these advantages, currently holographic projection does have limitations in biological imaging. The most challenging of these is the relatively slow response-time of the liquid crystal SLMs. As the voltage across a pixel is changed, there is a delay before the alignment of the liquid crystal cell will reach the desired orientation. For the SLM used, this response time and limited frame refresh rate meant acquisitions typically took 15s, limiting the live-cell imaging capabilities to slow-moving structures. However, with the latest generation of liquid-crystal SLMs offering considerably higher refresh rates than the transmission SLM used, imaging times could be significantly reduced. This longer imaging time also represents the worst-case scenario for imaging, where larger distances are required between excitation spots. In more sparsely labelled or thinner samples, where out-of-focus blur and excitation cross-talk is lowered, spot separation can be reduced, greatly lowering the number of pattern shifts required.

Funding

This project was funded by Durham University. RP acknowledges funding from the Royal Society University Research Fellowship. The authors declare no competing interests.

Acknowledgments

We would like to thank Mark Neil for providing a basic direct search algorithm and helpful discussion. We would also like to thank Andor for their very generous loan of the camera.

References

1. Gustafsson MG. (2000) Surpassing the lateral resolution limit by a factor of two using structured illumination microscopy. J. Microsc. 198:January. pp 82–7.
2. York AG, Parekh SH, Dalle Nogare D, et al. (2012) Resolution doubling in live, multicellular organisms via multifocal structured illumination microscopy. Nat. Methods 9:7. pp 749–54.
3. Ward EN, Pal R. (2017) Image scanning microscopy: an overview. J. Microsc. 266:2. pp 221–8.
4. Leach J, Sinclair G, Jordan P, et al. (2004) 3D manipulation of particles into crystal structures using holographic optical tweezers. Opt. Express 12:1. pp 220.
5. Sun B, Roichman Y, Grier DG, et al. (2008) Theory of holographic optical trapping. Opt. Express 16:20. pp 15765–76.
6. Grier DG. (2003,.) Nature.
7. Ward EN, Torkelsen FH, Pal R. (2018) Enhancing multi-spot structured illumination microscopy with fluorescence difference. R. Soc. Open Sci. 5:3. pp 171336.
8. Görlitz F, Guldbrand S, Runcorn TH, et al. (2018) easySLM-STED : Stimulated emission depletion microscopy with aberration correction , extended field of view and multiple beam scanning. :July. pp 1–11.

9. Curtis JE, Koss BA, Grier DG. (2002) Dynamic holographic optical tweezers. Opt. Commun. 207:1–6. pp 169–75.

10. Chakrova N, Rieger B, Stallinga S. (2016) Deconvolution methods for structured illumination microscopy. J. Opt. Soc. Am. A 33:7. pp B12–20.

11. N.Chakrova, B.Rieger SS. (2015) Studying different illumination patterns for resolution improvement in fluorescence microscopy. Opt. Express 23:24. pp 24692–701.

12. Soskind M, Soskind R, Soskind YG. (2010) Producing superresolved point-spread functions using a phase modulation technique. 7787. pp 77870T.

Fig. 1. SMF: Single-mode fibre. CL: Collimating lens. P1 & P2: Linear polarisers. QWP1 & QWP2: Quarter waveplates. SLM: Liquid-crystal spatial light modulator. RL1 & RL2: Relay lenses. DM: Long-pass dichroic mirror. OL: Objective lens. EF: Emission filter. TL: Tube lens.

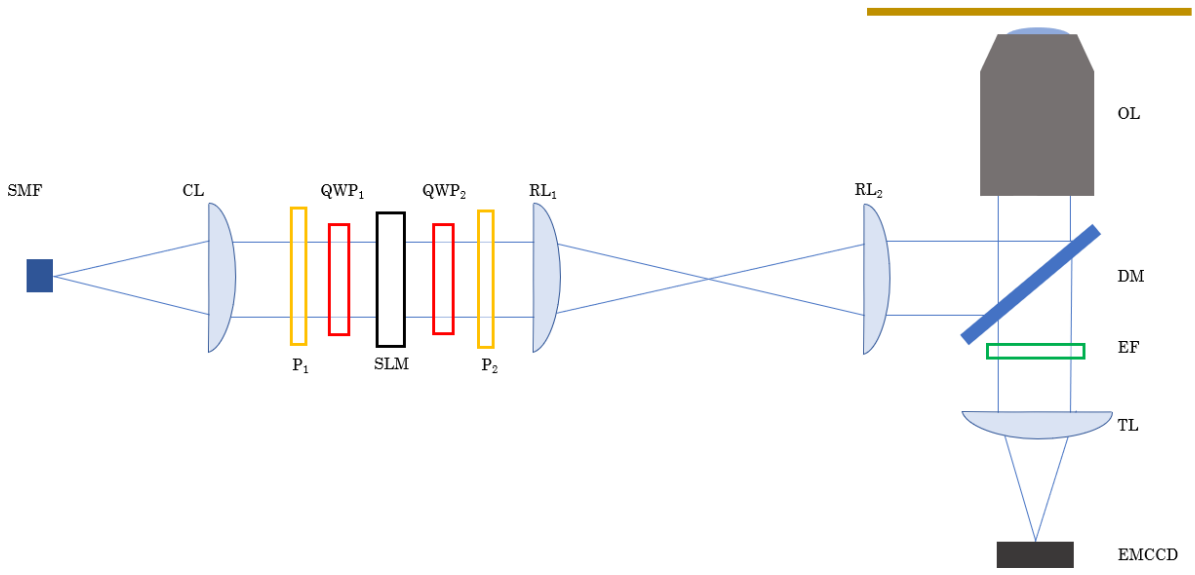

Fig. 2. Comparison of MSIM patterns generated with and without aberration correction. Left: MSIM pattern generated with no aberration correction. As well as intensity variation across the FOV, contrast is reduced as the PSFs are effective widened by the aberrations. Also apparent is that aberrations increase from the bottom right of the pattern to the top left. Right: Pattern projected after accounting for aberrations in the excitation optics. Not only is contrast increased by narrower PSFs, but also the shape of the PSFs remains unchanged across the FOV as location-dependant aberration correction has been used. In this pattering some intensity variation is still apparent though this less than would be expected from a similar FOV using the classical DMD approach.

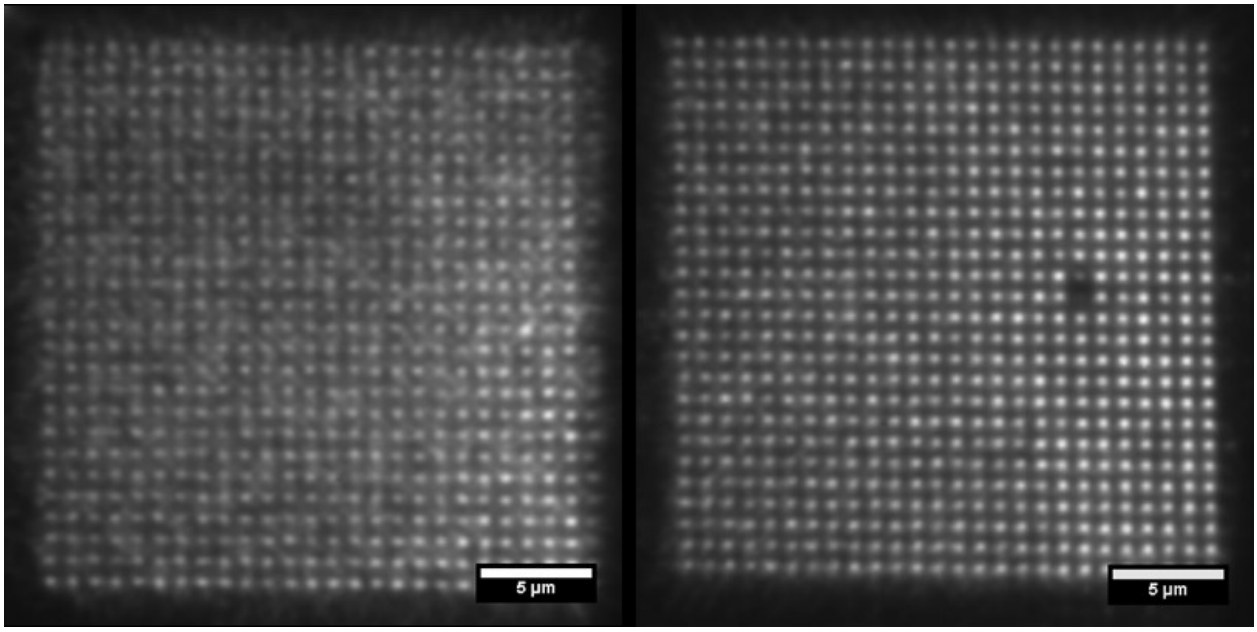

Fig. 3. MSIM imaging of fluorescent beads. Top left: Diffraction-limited image. Top right: MSIM image. Scale bar is 2.5 µm. Bottom: Intensity plot along blue line in both images. MSIM reconstruction was achieved with 5 PIFP iterations and 30 JRL iterations.

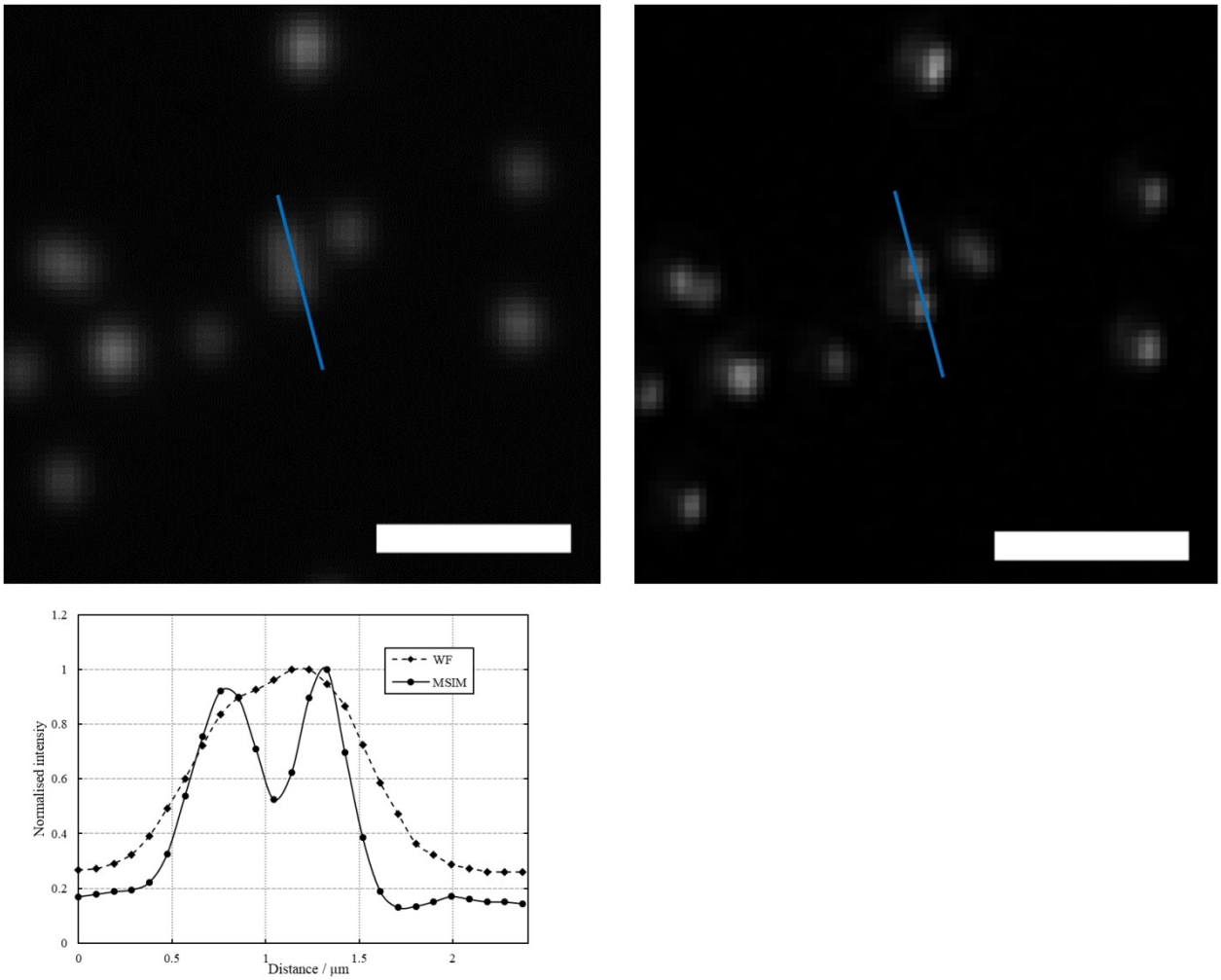

Fig. 4. MSIM imaging of actin cytoskeleton. Top Left: Diffraction-limited image. Top Right: MSIM image. Scale bar is 5 μm. Middle Left: Zoom of area of diffraction-limited image indicated in full FOV. Middle Right: Zoom of area of MSIM image. Scale bar is 1 μm. indicated in full FOV. Bottom: intensity plot along line shown in middle images. Dashed line is MSIM imaging and solid line is diffraction-limited imaging.

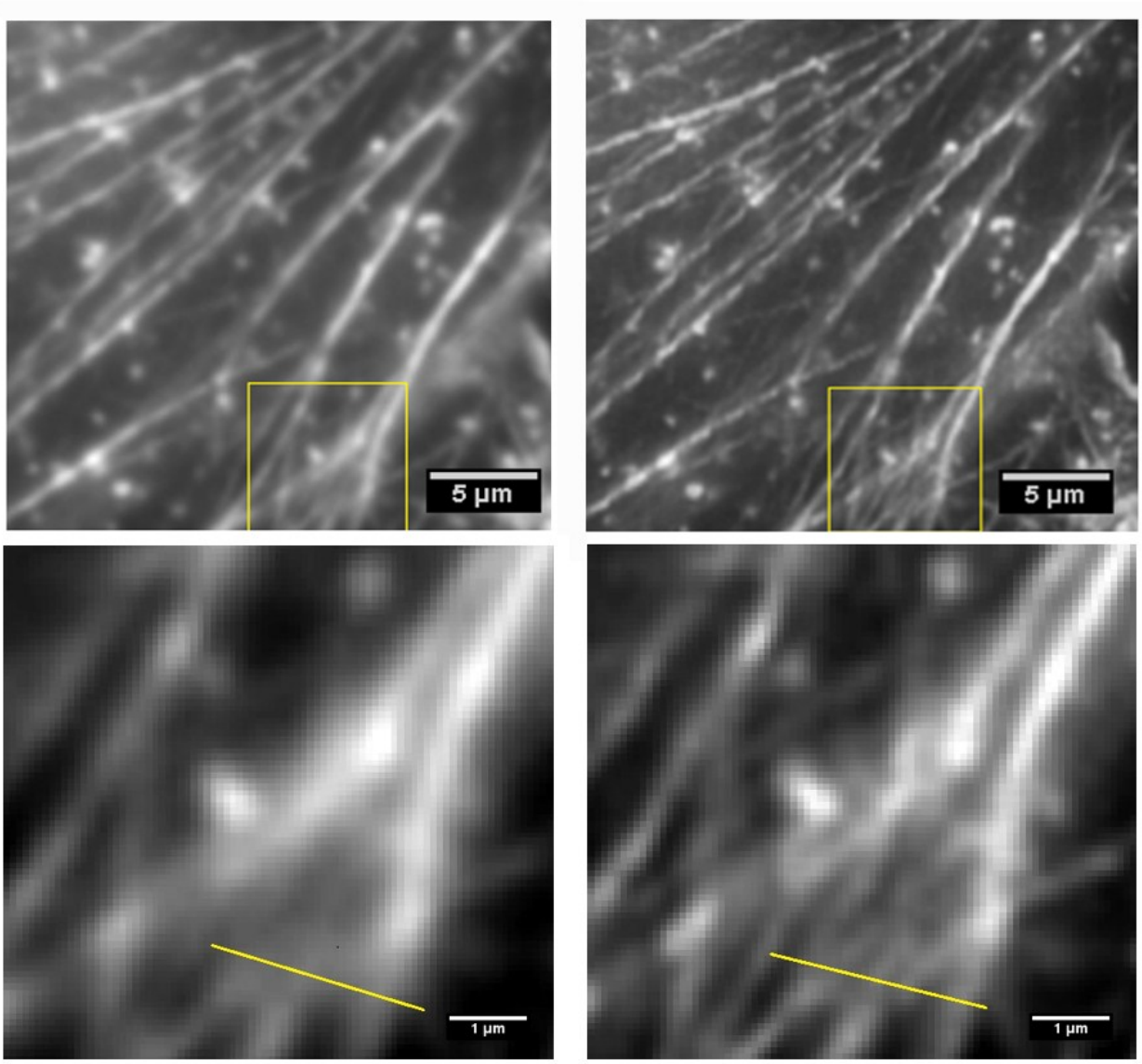

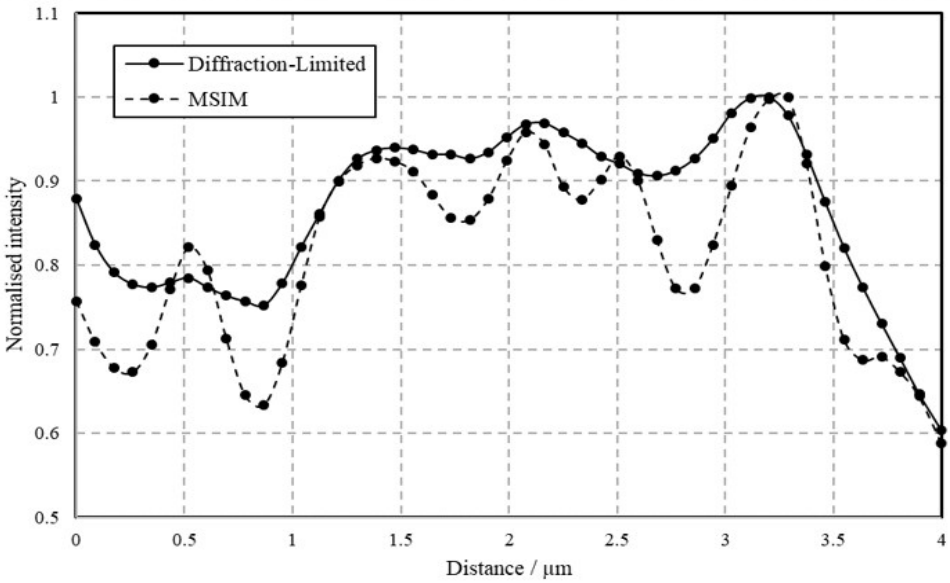

Fig. 5. MSIM imaging of the mitochondria in live cells. Left: Diffraction limited image. Right: MSIM image. Scale bar is 5μm. Reconstruction was achieved using 30 PIFP iterations and 30 JRL iterations.

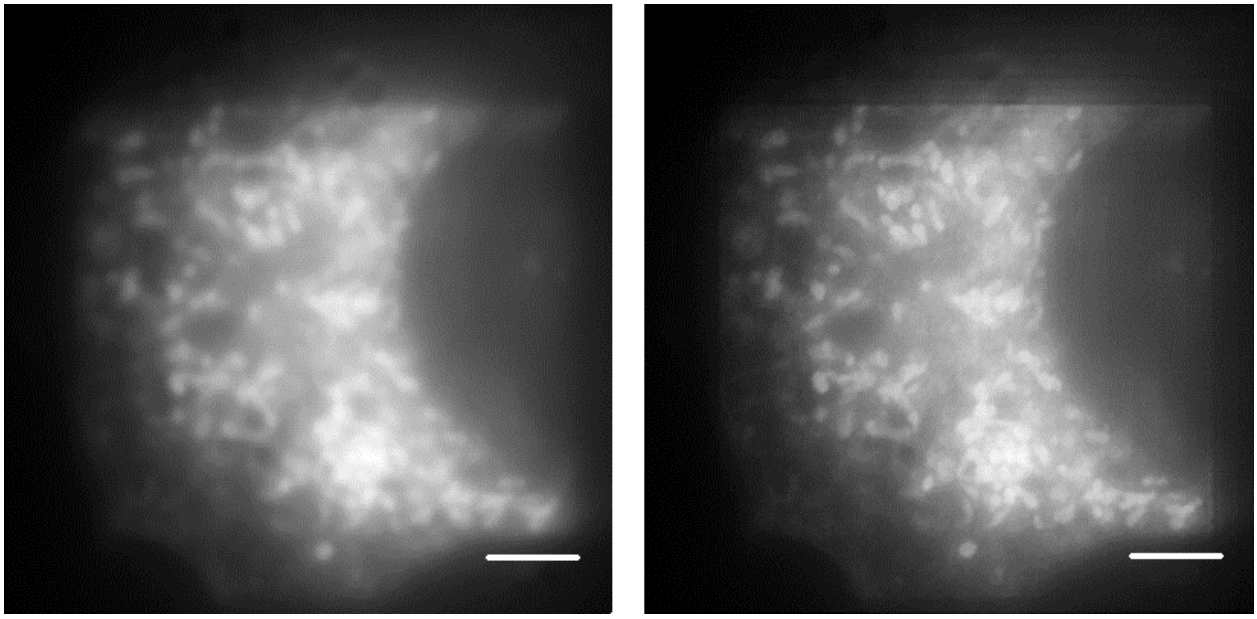

Fig. 6. Magnified regions of images shown in Fig. 4. Left: Diffraction-limited image. Right: MSIM reconstruction. Scale bars are 1 μm. Reconstruction was achieved using 30 PIFP iterations and 30 JRL iterations.